

Decay Studies of Exotic Nuclei using RISING and the GSI Fragment Separator

Spokesperson for the g-RISING collaboration: P.H.Regan
GSI contacts: J. Gerl & H.J. Wollersheim

This proposal forms part of the 'Stopped Beam' RISING experimental campaign at GSI.

PARTICIPANTS

CENBG Bordeaux, France: B. Blank
GSI-Darmstadt, Germany: J. Gerl, H.J. Wollersheim, F.Becker, H.Grawe, M.Gorska, P.Bednarczyk, N.Saitio, T.Saito
IKP Koeln, Germany: J. Jolie, P.Reiter
TU Munchen: R.Kruecken, T.Faestermann
University of Camerino, Italy: D. Balabanski, K. Gladnishki,
IFJ PAN Krakow, Poland: A.Maj
Warsaw University, Poland: M.Pfützner
Universidad Autonoma de Madrid, Spain: A.Jungclaus
Universidad de Santiago de Compostela, Spain: D.Cortina Gil, J.Benlliure, T. Kurtukian Nieto
IFIC Valencia, Spain: B. Rubio
INFN-Legnaro, Italy: A. Gadea, G.deAngelis,
University of Surrey, UK: Zs.Podolyák, P.H.Regan, P.M.Walker, W.Gelletly, W.N.Catford, Z.Liu, S. Williams
University of York, UK: M.A.Bentley, R.Wadsworth
University of Brighton, UK: A.M.Bruce
University of Manchester, UK: D.M.Cullen, S.J.Freeman
University of Liverpool, UK: R.D.Page
University of Edinburgh, UK: P.Woods, T.Davinson
CLRC Daresbury, UK: J.Simpson, D.Warner
Uppsala University, Sweden: H.Mach
Lund University, Sweden: D.Rudolph
Lawrence Berkeley National Lab, USA: R.M.Clark
University of Notre Dame, USA: M. Wiescher, A.Aprahamian
Debrecen, Hungary: A.Algora

for the STOPPED BEAM RISING COLLABORATION

Abstract: *We will investigate new structures in exotic, heavy neutron-rich and $N \sim Z$ nuclei formed following projectile fragmentation reactions using the Fragment Separator. The specific physics focus aims are:*

- *Investigating fundamental nuclear shell model interactions by identifying proton-hole states in the ^{208}Pb double-magic closed shell;*
- *The evolution of nuclear dynamical symmetries (and related nuclear shapes) from the extreme 'single-particle region' around ^{208}Pb towards the 'valence maximum' nucleus, ^{170}Dy ;*
- *The identification of isomeric states in proton-hole configurations in the ^{132}Sn doubly-closed core; and*
- *The study of isospin symmetry across the $N=Z$ line.*

The experimental technique involves the use of the FRagment Separator (FRS) at GSI to identify some of the most exotic, heavy nuclei synthesised to date. We will study the internal structure of these systems using γ -ray spectroscopy following: (i) the decay of metastable states (nuclear isomers) with lifetimes in the nano-to-millisecond time scale; and (ii) the β^- -decay of highly neutron-rich nuclei with ground state lifetimes in the seconds range. In both types of measurement, events will be time correlated with respect to the detection of individually identified nuclei at the final focus of the FRS. The capability for such experiments with fragments heavier than $A \sim 100$ is unique to the FRS. The proposed experiments will use the high-efficiency RISING γ -ray array of CLUSTER germanium detectors, complemented by BaF_2 detectors (which provide the opportunity for fast timing measurements in specific cases) and a segmented silicon 'active stopper' for β^- -decay measurements.

BACKGROUND

A major thrust of nuclear structure research is to determine and understand how the shell structure of nuclei changes for systems with highly asymmetric proton-to-neutron ratios. The proposed research for this portion of the *Stopped Beam RISING Experimental Campaign* will exploit radioactive beams, produced using projectile-fragmentation reactions to enable the first study of a range of highly exotic, heavy, neutron-rich nuclei. These will take advantage of the existence of nano-to-millisecond isomers in these nuclei to enable the first spectroscopic information to be obtained (more details on this technique from GSI-FRS-based work can be found in references [1-6]). The relatively low intensities of the secondary radioactive beams in such experiments (typically less than 1 ion per second) can often preclude the use of γ -ray coincidence measurements that are needed to confirm the nuclear decay schemes. However, isomeric decays and measurements of decays following β -emission can provide the vital γ -ray ‘fingerprints’ which give the first glimpses of excited states and the internal structure of such nuclei. A systematic study of key experimental signatures, such as the energy of the first excited state and/or of the ratio of the excitation energies of the lowest-lying levels in even-even nuclei, can vividly demonstrate the erosion of the established magic numbers. This reveals both new regions of nuclear shell structure and the development of nuclear collective excitations. The current proposal aims to identify such fingerprints following radioactive-beam studies in selected exotic nuclei using isomer and β^- -delayed γ -ray detection.

Figure 1 shows the predicted ground state nuclear decay modes as predicted by the Moller-Nix mass model [8]. While a very wide range of exotic nuclei can be populated in projectile fragmentation, in-beam spectroscopy of such systems (as performed in the ‘fast beam’ part of the RISING Campaign) is limited by the total germanium singles counting rate at the production target for the secondary radioactive ions. For very weakly produced secondary nuclei, this limitation makes their spectroscopy impossible at the current time, using the in-beam technique. However, by using the Fragment Separator to select and transport the specific nuclei of interest to the final focal plane of the FRS, decays from both isomeric states [1-6] and following the radioactive decay of the daughter nuclei can be performed [7], allowing the first spectroscopic information on these highly exotic systems.

*Moller Chart of Nuclides 2000
Decay Modes*

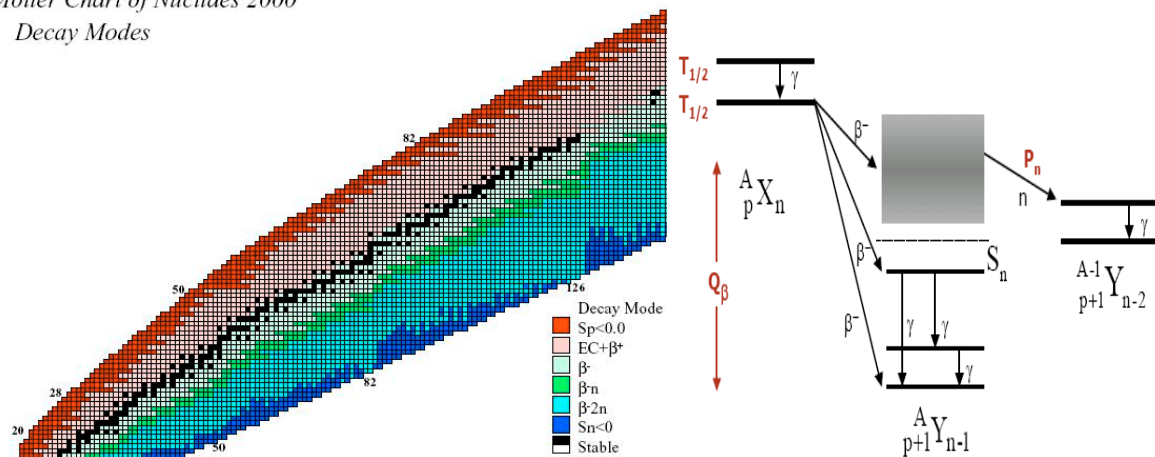


Figure 1: *Left:* Radioactive decay modes as predicted by the 2000 mass evaluation. *Right:* Schematic beta-decay and isomer modes of decay to populate excited states in specific daughter nuclei.

The specific stopped beam proposals are presented following a meeting to discuss the specific physics aims of the Stopped Beam RISING campaign, which took place at the University of Surrey in March 2004 (see http://www.ph.surrey.ac.uk/~phs1pr/rising/stopped_workshop_04). Note that the proposals submitted in this, ‘active stopper’ phase of the stopped beam RISING campaign are complemented by a series of proposals aimed at measuring gyromagnetic ratios of isomeric states using a similar, but not identical, set-up (see proposals by G.Neyens et al.,).

be placed in the gamma-ray array for the ‘fast-timing’ of lifetimes in the hundreds of pico to few nanoseconds time range. This may also be utilised in specific cases where the ordering of newly observed transitions in a cascade needs to be measured.

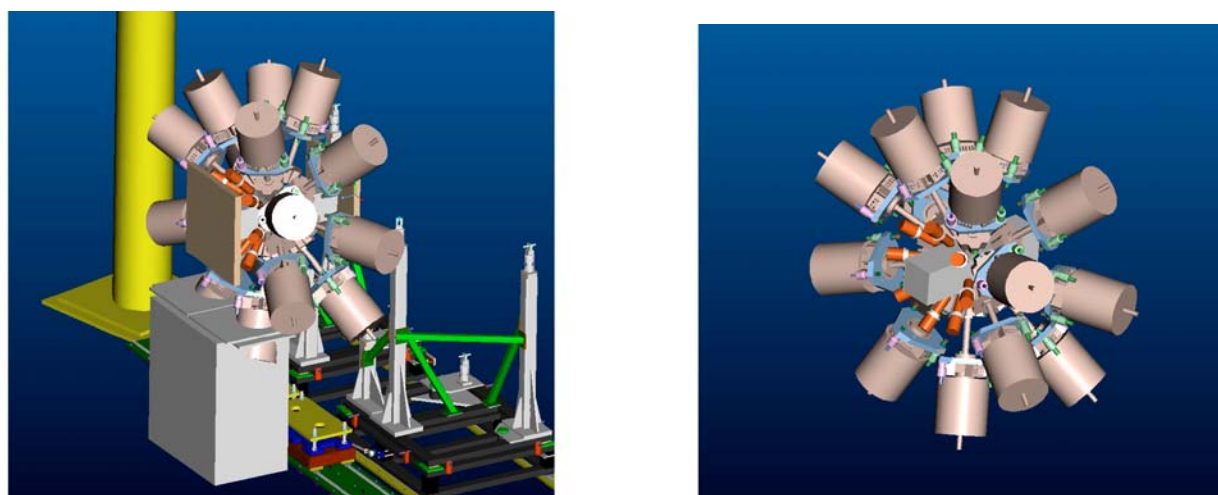


Figure 3 CAD drawings of the Stopped Beam RISING array, plus 8 BAF2 detectors for fast timing placed at forward angles. (left) Showing the support structure and space/plates for fast plastic scintillation detectors and (right) Shows space for the 25cm x 25cm vacuum chamber in which to house the DSSSDs.

The FRS will be used in the monochromatic mode which will enable specific ions to be stopped in a single 1mm thick silicon detector. This means that the experimenters can select specific elements of interest for β -delayed study. Figure 4 shows the effect of this from the recent experiment of Benlliure et al., following the fragmentation of a ^{208}Pb beam on a ^9Be target at a beam energy of 1 GeV per nucleon.

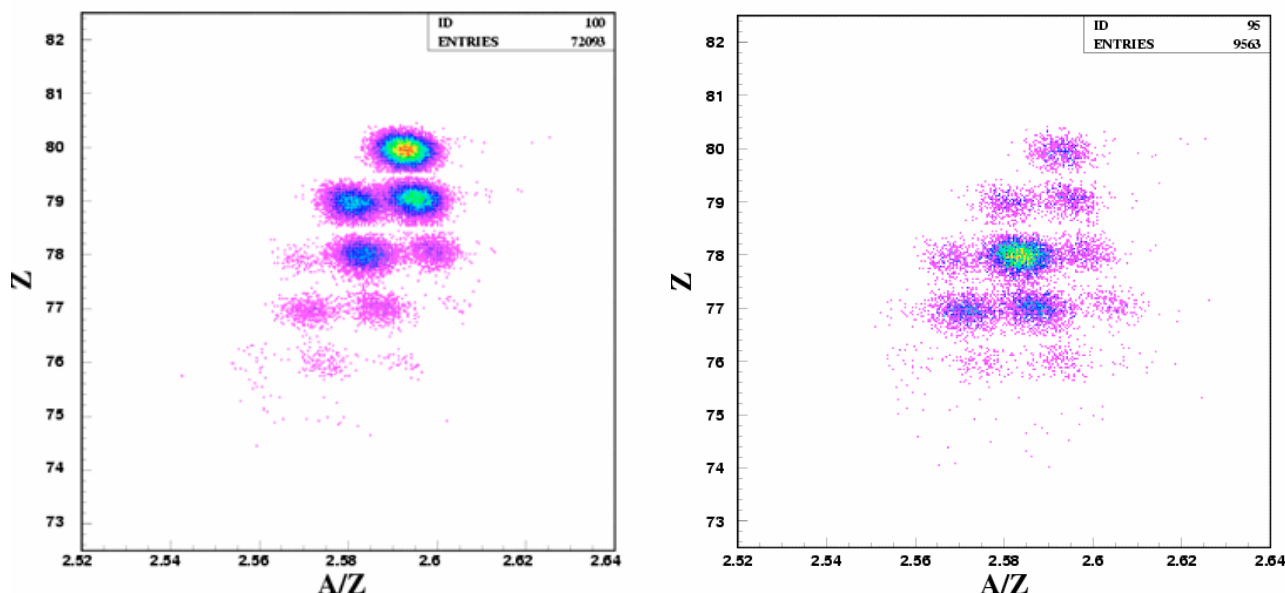


Figure 4 Particle identification plots centred on ^{198}Ir ions produced following the fragmentation of 1 GeV per nucleon ^{208}Pb beam on a ^9Be target with the FRS used in monochromatic mode. The left hand figure shows the total production yield at the end of the FRS, while the right hand side is limited to those ions which stopped in the 1mm thick silicon detector.

The active stopper will consist of three 5cm by 5cm double sided silicon strip detectors (DSSSDs) each with 16 horizontal and 16 vertical strips (giving each detector defined 256 pixels, or 768 pixels for the active stopper as a whole). The active stopper detectors are 1 mm thick, which is enough to stop all the ions of a given element if the FRS is used in monochromatic mode. (Heavier elements are stopped in the

degrader or plastic scintillator which precedes the active stopper, as shown schematically on the left hand side of figure 2, while the lower-Z elements pass through the active stopper and are detected in to the plastic veto scintillator detector.

A number of the proposed experiments for the Active Stopper RISING campaign rely on rate estimates assuming ‘cold fragmentation’ of the primary beam [12]. Figure 5 shows the robustness of these estimates when compared with the measured cross-sections for cold-fragmentation products following reactions between a ^{197}Au beam on ^9Be target at 950 MeV per nucleon [12].

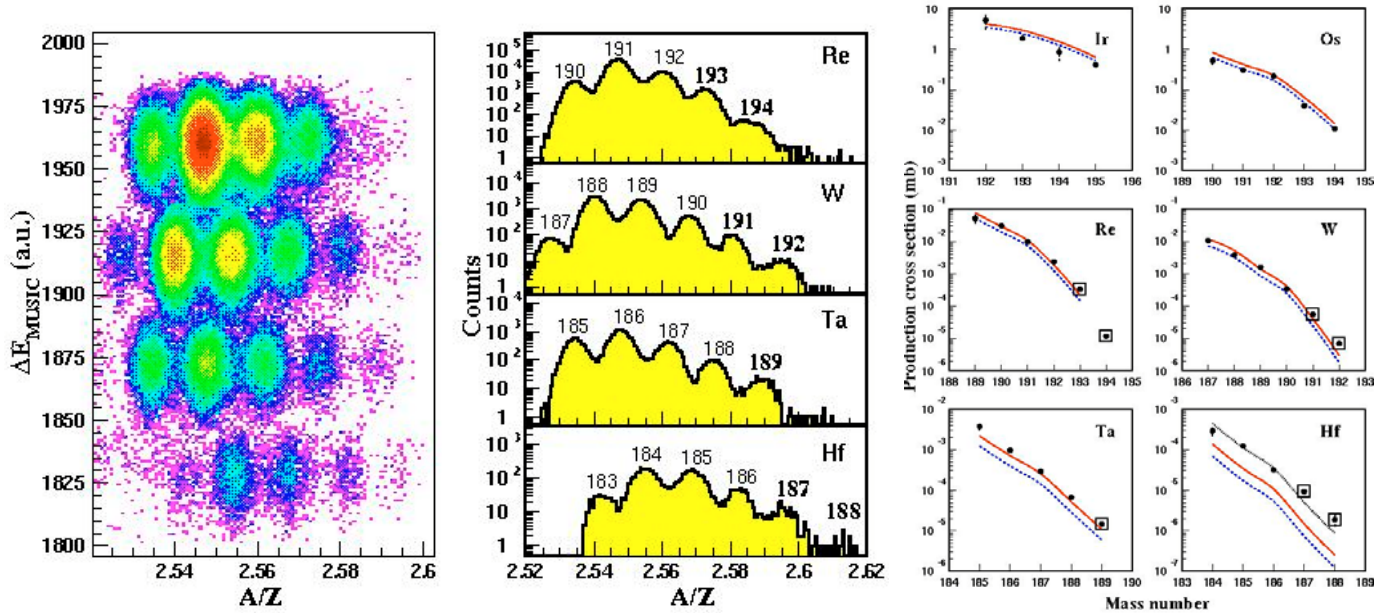


Figure 5: Particle identification plots and experimental cross-sections for the ‘cold fragmentation’ products in the $^{197}\text{Au}+^9\text{Be}$ reaction, highlighting the good agreements with the theoretical predictions for the cross-section given in reference. (Data taken from ref. [12]).

Assuming upper-limit β -decay half-life measurements of up to 30 seconds for the less exotic nuclei such as $^{204,5}\text{Au}$, [11], this implies each pixel can be hit by a new ion on average every 150 seconds (5 typical half-lives) for a reasonable peak to total ratio. This assumption leads to a maximum implantation rate at the active stopper of around 5 ions in total per second, or 144k per 8 hour shift. The DSSSD array will have dual gain pre-amplifiers to obtain energy measurements for both the implanted heavy ion and the subsequently emitted β -particle. Each event will be time stamped with a MHz clock to allow time correlation between the implantation and the subsequent β -decay in the same pixel. Most of the nuclei of interest have predicted β -decay half-lives of less than 10 seconds (see figures 6-9) which should significantly improve the experimentally useful correlation-time limit.

TIMELINESS

The proposal precedes a massive investment in the GSI-FAIR facility. This €700M upgrade will make GSI the world’s leading laboratory to study heavy, radioactive nuclei. This proposal represents a unique opportunity for the nuclear structure community to build on its initial projectile fragmentation isomer and reaction work at GSI and to drive a major physics initiative in nuclear spectroscopy through the RISING project. The combination of the FRS and the RISING array mean that the experimental technology is only now available to enable the measurements outlined in the following proposals.

91	Pa215 0.844s	Pa216 0.167s	Pa217 0.832s	Pa218 0.88227s	Pa219 0.898s	Pa220 0.898s	Pa221 0.898s	Pa222 0.898s	Pa223 0.898s	Pa224 0.898s	Pa225 0.898s	Pa226 0.898s	Pa227 0.898s	Pa228 0.898s	Pa229 0.898s
90	Th214 0.1s	Th215 1.2s	Th216 0.627s	Th217 0.88167s	Th218 1.87e-07s	Th219 0.898s	Th220 0.898s	Th221 0.898s	Th222 0.898s	Th223 0.898s	Th224 0.898s	Th225 0.898s	Th226 0.898s	Th227 0.898s	Th228 0.898s
89	Ac213 0.731s	Ac214 0.731s	Ac215 0.731s	Ac216 0.80044s	Ac217 0.731s	Ac218 0.731s	Ac219 0.731s	Ac220 0.731s	Ac221 0.731s	Ac222 0.731s	Ac223 0.731s	Ac224 0.731s	Ac225 0.731s	Ac226 0.731s	Ac227 0.731s
88	Ra212 0.1s	Ra213 0.1s	Ra214 0.1s	Ra215 0.1s	Ra216 0.1s	Ra217 0.1s	Ra218 0.1s	Ra219 0.1s	Ra220 0.1s	Ra221 0.1s	Ra222 0.1s	Ra223 0.1s	Ra224 0.1s	Ra225 0.1s	Ra226 0.1s
87	Fr211 3.1s	Fr212 2.8s	Fr213 3.1s	Fr214 3.1s	Fr215 3.1s	Fr216 3.1s	Fr217 3.1s	Fr218 3.1s	Fr219 3.1s	Fr220 3.1s	Fr221 3.1s	Fr222 3.1s	Fr223 3.1s	Fr224 3.1s	Fr225 3.1s
86	Rn210 2.42s	Rn211 14.6h	Rn212 22.8s	Rn213 0.195s	Rn214 0.195s	Rn215 0.195s	Rn216 0.195s	Rn217 0.195s	Rn218 0.195s	Rn219 0.195s	Rn220 0.195s	Rn221 0.195s	Rn222 0.195s	Rn223 0.195s	Rn224 0.195s
85	At209 0.91h	At210 0.91h	At211 0.91h	At212 0.91h	At213 0.91h	At214 0.91h	At215 0.91h	At216 0.91h	At217 0.91h	At218 0.91h	At219 0.91h	At220 0.91h	At221 0.91h	At222 0.91h	At223 0.91h
84	Po208 0.199e+1s	Po209 0.199e+1s	Po210 0.199e+1s	Po211 0.199e+1s	Po212 0.199e+1s	Po213 0.199e+1s	Po214 0.199e+1s	Po215 0.199e+1s	Po216 0.199e+1s	Po217 0.199e+1s	Po218 0.199e+1s	Po219 0.199e+1s	Po220 0.199e+1s	Po221 0.199e+1s	Po222 0.199e+1s
83	Bi207 0.199e+1s	Bi208 0.199e+1s	Bi209 0.199e+1s	Bi210 0.199e+1s	Bi211 0.199e+1s	Bi212 0.199e+1s	Bi213 0.199e+1s	Bi214 0.199e+1s	Bi215 0.199e+1s	Bi216 0.199e+1s	Bi217 0.199e+1s	Bi218 0.199e+1s	Bi219 0.199e+1s	Bi220 0.199e+1s	Bi221 0.199e+1s
82	Pb206 24.1h	Pb207 22.1h	Pb208 52.4h	Pb209 3.253h	Pb210 22.3s	Pb211 36.1h	Pb212 10.64h	Pb213 19.2h	Pb214 26.8h	Pb215 36s	Pb216 38.7s	Pb217 28.7s	Pb218 14.5s	Pb219 5.94s	Pb220 0.479s
81	Tl205 38.47s	Tl206 4.199s	Tl207 4.27h	Tl208 3.853s	Tl209 2.151h	Tl210 1.3h	Tl211 4.18s	Tl212 2.89s	Tl213 1.45s	Tl214 1.22s	Tl215 0.811s	Tl216 0.63s	Tl217 0.479s	Tl218 0.44s	Tl219 0.44s
80	Hg204 0.87h	Hg205 0.87h	Hg206 0.87h	Hg207 0.87h	Hg208 0.87h	Hg209 0.87h	Hg210 0.87h	Hg211 0.87h	Hg212 0.87h	Hg213 0.87h	Hg214 0.87h	Hg215 0.87h	Hg216 0.87h	Hg217 0.87h	Hg218 0.87h
79	Au203 1h	Au204 39.5s	Au205 31s	Au206 1.59s	Au207 1.3s	Au208 1.29s	Au209 0.746s	Au210 0.917s	Au211 0.587s	Au212 0.411s	Au213 0.32s	Au214 0.267s	Au215 0.196s	Au216 0.196s	Au217 0.196s
78	Pt202 18.3s	Pt203 6.75s	Pt204 0.674s	Pt205 0.465s	Pt206 0.562s	Pt207 0.302s	Pt208 0.379s	Pt209 0.179s	Pt210 0.177s	Pt211 0.177s	Pt212 0.177s	Pt213 0.177s	Pt214 0.177s	Pt215 0.177s	Pt216 0.177s
77	Ir201 18.3s	Ir202 8.3s	Ir203 3.88s	Ir204 0.48s	Ir205 0.256s	Ir206 0.256s	Ir207 0.187s	Ir208 0.288s	Ir209 0.124s	Ir210 0.124s	Ir211 0.124s	Ir212 0.124s	Ir213 0.124s	Ir214 0.124s	Ir215 0.124s
76	Os200 1.94s	Os201 1.23s	Os202 0.535s	Os203 0.116s	Os204 0.895s	Os205 0.114s	Os206 0.114s	Os207 0.114s	Os208 0.114s	Os209 0.114s	Os210 0.114s	Os211 0.114s	Os212 0.114s	Os213 0.114s	Os214 0.114s
75	Re199 1.94s	Re200 1.23s	Re201 0.535s	Re202 0.116s	Re203 0.895s	Re204 0.114s	Re205 0.114s	Re206 0.114s	Re207 0.114s	Re208 0.114s	Re209 0.114s	Re210 0.114s	Re211 0.114s	Re212 0.114s	Re213 0.114s

Figure 6: Predicted (white squares) β -decay half-lives for the neutron-rich N~126 region [9].

83	Bi193 1.14h	Bi194 1.95s	Bi195 3.85s	Bi196 3.13s	Bi197 3.33s	Bi198 11.6h	Bi199 27s	Bi200 36.4h	Bi201 1.9h	Bi202 1.72h	Bi203 11.7h	Bi204 11.57h	Bi205 45.81s	Bi206 6.236s	Bi207 31.95s
82	Pb192 3.5m	Pb193 5.8m	Pb194 18s	Pb195 15m	Pb196 37m	Pb197 43m	Pb198 2.4h	Pb199 1.5h	Pb200 21.5h	Pb201 9.33h	Pb202 5.75e+04s	Pb203 2.161d	Pb204 1.4d	Pb205 1.15e+07s	Pb206 24.1h
81	Tl191 5.22m	Tl192 18.8m	Tl193 21.6m	Tl194 33s	Tl195 1.16h	Tl196 1.84h	Tl197 2.84h	Tl198 5.3h	Tl199 7.42h	Tl200 1.95d	Tl201 3.838d	Tl202 12.23d	Tl203 29.32d	Tl204 3.78h	Tl205 78.47h
80	Hg190 28.7m	Hg191 42.5m	Hg192 3.88h	Hg193 17.65h	Hg194 0.527d	Hg195 1.73d	Hg196 2.786d	Hg197 9.37d	Hg198 15.87d	Hg199 23.1d	Hg200 13.13d	Hg201 25.96d	Hg202 45.61d	Hg203 6.97d	Hg204 18.3d
79	Au189 19.2d	Au190 18.77h	Au191 0.441d	Au192 2.852d	Au193 0.797d	Au194 0.99d	Au195 52.537d	Au196 59.837d	Au197 25.242d	Au198 10.85m	Au199 7.165s	Au200 30.5m	Au201 12.5h	Au202 2.9m	Au203 1.64s
78	Pt188 10.5h	Pt189 1.73d	Pt190 13.2d	Pt191 11.78d	Pt192 37.3d	Pt193 241v	Pt194 62.7d	Pt195 171d	Pt196 3.8h	Pt197 1.4h	Pt198 8.7m	Pt199 8s	Pt200 1.61h	Pt201 13.3s	Pt202 18.5s
77	Ir187 10.5h	Ir188 1.73d	Ir189 13.2d	Ir190 11.78d	Ir191 37.3d	Ir192 241v	Ir193 62.7d	Ir194 171d	Ir195 3.8h	Ir196 1.4h	Ir197 8.7m	Ir198 8s	Ir199 1.61h	Ir200 13.3s	Ir201 18.5s
76	Os186 1.89s	Os187 1.9s	Os188 13.2d	Os189 15.15d	Os190 26.2d	Os191 15.4d	Os192 40.7h	Os193 1.295d	Os194 6.5m	Os195 84.9m	Os196 1.36h	Os197 45.5s	Os198 17.2s	Os199 16s	Os200 16s
75	Re185 37.4s	Re186 28.95s	Re187 52.4s	Re188 1.95d	Re189 3.2h	Re190 9.3h	Re191 1.69d	Re192 18.1s	Re193 18.3s	Re194 18.3s	Re195 5.162s	Re196 5.131s	Re197 5.162s	Re198 5.131s	Re199 1.34s
74	W184 30.64s	W185 28.64s	W186 28.64s	W187 22.33s	W188 11.76s	W189 11.76s	W190 1.16h	W191 36.36s	W192 21s	W193 8.889s	W194 6.16s	W195 4.79s	W196 2.13s	W197 1.32s	W198 1.32s
73	Ta183 5.1d	Ta184 8.7h	Ta185 49.4h	Ta186 18.5m	Ta187 1.82m	Ta188 24.1s	Ta189 34.2s	Ta190 8.51s	Ta191 9.52s	Ta192 4.42s	Ta193 2.86s	Ta194 1.5s	Ta195 1.62s	Ta196 0.768s	Ta197 0.577s
72	Hf182 9.3e+06s	Hf183 1.067h	Hf184 4.12h	Hf185 3.5m	Hf186 2.6m	Hf187 11.7s	Hf188 6.39s	Hf189 5.39s	Hf190 4.2s	Hf191 2.62s	Hf192 1.22s	Hf193 1.04s	Hf194 0.726s	Hf195 0.454s	Hf196 0.298s
71	Lu181 3.5m	Lu182 2.4m	Lu183 38s	Lu184 18s	Lu185 6.75s	Lu186 3.88s	Lu187 4.96s	Lu188 2.11s	Lu189 2.16s	Lu190 1.13s	Lu191 0.65s	Lu192 0.625s	Lu193 0.475s	Lu194 0.298s	Lu195 0.298s
70	Yb180 2.4m	Yb181 4.88s	Yb182 3.38s	Yb183 1.87s	Yb184 2.01s	Yb185 0.733s	Yb186 0.594s	Yb187 0.559s	Yb188 0.349s	Yb189 0.312s	Yb190 0.245s	Yb191 0.182s	Yb192 0.182s	Yb193 0.182s	Yb194 0.182s
69	Tm179 4.88s	Tm180 3.38s	Tm181 1.87s	Tm182 2.01s	Tm183 0.733s	Tm184 0.594s	Tm185 0.559s	Tm186 0.349s	Tm187 0.312s	Tm188 0.245s	Tm189 0.182s	Tm190 0.182s	Tm191 0.182s	Tm192 0.182s	Tm193 0.182s
68	Er178 1.64s	Er179 1.65s	Er180 0.8s	Er181 0.984s	Er182 0.321s	Er183 0.383s	Er184 0.261s	Er185 0.21s	Er186 0.21s	Er187 0.21s	Er188 0.21s	Er189 0.21s	Er190 0.21s	Er191 0.21s	Er192 0.21s
67	Hol77 0.711s	Hol78 0.607s	Hol79 0.35s	Hol80 0.403s	Hol81 0.171s	Hol82 0.167s	Hol83 0.15s	Hol84 0.13s	Hol85 0.13s	Hol86 0.13s	Hol87 0.13s	Hol88 0.13s	Hol89 0.13s	Hol90 0.13s	Hol91 0.13s

Figure 7 Predicted (white squares) β -half-lives for the ¹⁹⁰W Region [9].

71	Lu167 51.5m	Lu168 6.7h	Lu169 1.42d	Lu170 2.012d	Lu171 8.24d	Lu172 6.7d	Lu173 1.37d	Lu174 3.31v	Lu175 97.41	Lu176 2.53	Lu177 160.4d	Lu178 28.4h	Lu179 4.59h	Lu180 5.7m	Lu181 3.5m
70	Yb166 2.36d	Yb167 17.5m	Yb168 0.13	Yb169 32.83d	Yb170 3.94	Yb171 14.28	Yb172 21.83	Yb173 16.13	Yb174 31.83	Yb175 0.185d	Yb176 12.7s	Yb177 1.911h	Yb178 1.23h	Yb179 8m	Yb180 2.4m
69	Tm165 1.255d	Tm166 7.7h	Tm167 5.25d	Tm168 39.1d	Tm169 188	Tm170 178.6d	Tm171 11.92d	Tm172 1.65d	Tm173 9.24h	Tm174 5.4h	Tm175 185.2h	Tm176 1.3h	Tm177 1.42m	Tm178 4.88s	Tm179 1.64s
68	Er164 1.61d	Er165 37.5m	Er166 36.41	Er167 22.33	Er168 35.39	Er169 0.6d	Er170 14.35	Er171 7.516d	Er172 2.85d	Er173 1.4h	Er174 3.1h	Er175 1.76h	Er176 5.78h	Er177 4.07s	Er178 1.64s
67	Hol163 4570s	Hol164 37.5m	Hol165 190	Hol166 1290h	Hol167 3.1h	Hol168 2.39m	Hol169 4.7h	Hol170 2.76m	Hol171 53s	Hol172 75s	Hol173 7.3s	Hol174 4.15s	Hol175 1.69s	Hol176 1.23s	Hol177 0.711s
66	Dy162 25.51	Dy163 24.9	Dy164 28.18	Dy165 2.324h	Dy166 3.4d	Dy167 6.2m	Dy168 9.7h	Dy169 39s	Dy170 19.7s	Dy171 6.8s	Dy172 4.83s	Dy173 1.68s	Dy174 0.916s	Dy175 0.903s	Dy176 0.419s
65	Tb161 6.88d	Tb162 7.6m	Tb163 19.9m	Tb164 3m	Tb165 2.11s	Tb166 29.6s	Tb167 19.4s	Tb168 8.2s	Tb169 2.35s	Tb170 1.97s	Tb171 0.892s	Tb172 0.772s	Tb173 0.471s	Tb174 0.366s	Tb175 0.281s
64	Gd160 21.8s	Gd161 3.66m	Gd162 9.4m	Gd163 1.13m	Gd164 49s	Gd165 10.2s	Gd166 4.8s	Gd167 0.91s	Gd168 1.36s	Gd169 1.08s	Gd170 0.48s	Gd171 0.418s	Gd172 0.226s	Gd173 0.216s	Gd174 0.118s
63	Eu159 18.1h	Eu160 79s	Eu161 26s	Eu162 18.6s	Eu163 6.67s	Eu164 2.46s	Eu165 1.59s	Eu166 0.996s	Eu167 0.925s	Eu168 0.525s	Eu169 0.231s	Eu170 0.21s	Eu171 0.139s	Eu172 0.139s	Eu173 0.0779s
62	Sm158 9.3h	Sm159 11.37s	Sm160 3.64	Sm161 4.8s	Sm162 1.89s	Sm163 1.39s	Sm164 0.521s	Sm165 0.69s	Sm166 0.296s	Sm167 0.211s	Sm168 0.12s	Sm169 0.125s	Sm170 0.125s	Sm171 0.125s	Sm172 0.125s
61	Pm157 10.56s	Pm158 4.8s	Pm159 1.47s	Pm160 2.45s	Pm161 0.863s	Pm162 0.583s	Pm163 0.321s	Pm164 0.233s	Pm165 0.14s	Pm166 0.132s	Pm167 0.0871s	Pm168 0.0902s	Pm169 0.0902s	Pm170 0.0902s	Pm171 0.0902s
60	Nd156 5.47s	Nd157 2.72s	Nd158 0.862s	Nd159 0.794s	Nd160 0.274s	Nd161 0.258s	Nd162 0.124s	Nd163 0.108s	Nd164 0.0537s	Nd165 0.0537s	Nd166 0.0537s	Nd167 0.0537s	Nd168 0.0537s	Nd169 0.0537s	Nd170 0.0537s
59	Pr155 0.772s	Pr156 0.979s	Pr157 0.47s	Pr158 0.424s	Pr159 0.22s	Pr160 0.195s	Pr161 0.085s	Pr162 0.093s	Pr163 0.0513s	Pr164 0.0513s	Pr165 0.0513s	Pr166 0.0513s	Pr167 0.0513s	Pr168 0.0513s</	

